Single Crystal Charge Density Studies of Thermoelectric Material Indium Antimonide

Muthaian Charles Robert[a], Bandarinathan Subha[b], and Ramachandran Saravanan[b]

[a] Department of Physics, H.K.R.H. College, Uthamapalayam – 625 533, Tamil Nadu, India
[b] Research Centre and PG Department of Physics, The Madura College, Madurai – 625 011, Tamil Nadu, India

Reprint requests to R. S.; E-mail: saragow@dataone.in

Z. Naturforsch. **66a,** 562 – 568 (2011) / DOI: 10.5560/ZNA.2011-0004
Received January 25, 2011 / revised February 24, 2011

The average structure of the thermoelectric material indium antimonide (InSb) has been studied in terms of the electron density distribution using the single crystal X-ray intensity data. The charge density of this material has been studied including and excluding the quasi-forbidden $h+k+l=4n+2$ type reflections using the maximum entropy method (MEM). Both the pictorial and numerical results of the experimental electron density show mixed ionic and covalent character in InSb. The use of InSb as a thermoelectric material is supported through charge density analysis.

Key words: Electron Density; InSb; Local Structure; Thermoelectric; XRD; MEM.

1. Introduction

Environmentally green and efficient power sources are the emerging needs of the future technology. Thermoelectric materials fit well this character by changing heat into electricity isentropically using the Seebeck and Peltier cooling effects. Thermoelectric materials can cool up to hundreds of degrees and handle large heat fluxes for a given applied voltage. In addition, electrical power ranging from microwatts to watts can be produced in a thermoelectric material. Miniaturized radioisotope solid-state power sources were designed and are in use for the past few decades [1]. Since thermoelectrics are made of solid-state materials, they have no moving parts and do not undergo chemical reactions. However, they still do not have high enough efficiencies to be viable in many commercial fields, such as domestic air conditioning and waste heat recovery. Most contemporary research in thermoelectric materials deals with developing compounds and devices with greater efficiency. Currently, there is a strong impetus towards identifying thermoelectric materials with the thermoelectric figure of merit greater than unity ($ZT > 1$). The challenge in these efforts lies in achieving simultaneously high electrical conductivity, high thermoelectric power, and low thermal conductivity in the same solid. These properties define the thermo electric figure of merit $ZT = S^2\sigma T/k$, where, S is the Seebeck coefficient, σ is the electrical conductivity, k is the thermal conductivity, and T is the absolute temperature. The quantities S and σ are determined by the details of the electronic structure and scattering of charge carriers (electronic and holes) and thus are not independently controllable parameters. The thermal conductivity k has a contribution from lattice vibrations k_l as well as from electronic charge carries k_e, thus $k = k_e + k_l$. Therefore, one way to increase ZT is to minimize k_l while retaining good electrical and thermo power properties, called phonon glass electron crystal (PGEC) [2].

The emerging families of advanced thermoelectric materials are dominated by antimonides and tellurides. Because the structures of the tellurides are mostly composed of NaCl-related motifs, they do not contain any Te–Te bonds, and all of the antimonide structures exhibit Sb–Sb bonds of various lengths [3]. Thermoelectric properties of InSb nanowire grown using a vapour–liquid–solid method has been reported by Seol et al. [4].

While InSb is mainly used as infrared detectors and Hall sensors [5], studies have shown that InSb has much potential as thermoelectric devices [6]. It is reported that the Seebeck coefficient and the power factor for Si-doped and undoped InSb thin films

are $-214\,\mu V/K$, $-261\,\mu V/K$ and $2\cdot10^{-4}\,W/mK^2$, $1.3\cdot10^{-3}\,W/mK^2$. Further, the thermoelectric properties of GaSb and InSb alloys were studied and reported [7].

Since InSb is reported as to be a good thermoelectric material, the structural information along with the electron density distribution is essential to characterize this material, besides all its experimental observations. Hence, the present work is aimed at the structural analysis of the single crystal X-ray data of InSb in terms of the electron density distribution between atoms using the maximum entropy method (MEM) [8]. The refinement of the structure was carried out using software which also can be used for Rietveld [9] type refinements.

The qualitative and quantitative electron distribution of the atoms in crystalline materials were studied using the maximum entropy formalism, because it provides less biased information on the electron densities of the crystals compared to conventional Fourier synthesis [10 – 12].

2. Experiment

Small spheres of InSb crystals were prepared from bulk crystals using a home-made crystal spherizer and the strained surface was etched with suitable solutions so as to attain perfect spherical nature with little tolerance. A good quality single crystal sphere as shown in Figure 1 with radius 0.0605(10) mm was chosen and single crystal X-ray diffraction data were collected using a CAD-4 X-ray diffractometer with Mo K_α X-radiation and graphite as the monochromator. The data set was collected with several psi-scan sets resulting in the transmission factor of about 1.

Fig. 1 (colour online). Single crystal InSb sphere used for X-ray data collection (sphere radius 0.0605(10) mm).

Three standard reflections were monitored for every two hours ($0.99 <$ decay < 1.0056) and a total of 867 reflections were measured. The quasi-forbidden reflections of the type $h+k+l=4n+2$ were also measured. Among these 867 reflections, 257 reflections are of $h+k+l=4n+2$ type. The cell refinement has been done within a θ range of 6.00° to 16.96°. InSb belongs to a cubic structure with space group F-43m (zinc blende structure). There are four molecules/cell at special positions 4(a) and 4(c). The refined cell constant is 6.463(6) Å.

3. Refinements

3.1. Rietveld Refinements

The raw intensity data set of the single crystal sphere of InSb was corrected for absorption. The μR value turned out to be 1.1. The absorption corrected data set was refined using the software package JANA 2006 [13]. Table 1 represents the refined structure factors with $\sigma(F_o)$ values after the final refinements. The reliability indices of these refinements are very low ($R_{obs} = 2.92\%$ and $wR_{obs} = 4.99\%$).

The allowed reflections for InSb are $h+k+l=4n$, $h+k+l=4n\pm1$, and $h+k+l=4n+2$, where n is an integer. Among these type of reflections, the $h+k+l=4n+2$ type reflections will be very weak and are called quasi-forbidden reflections. The theoretical structure factor expression for the quasi-forbidden, $h+k+l=4n+2$ type reflections is given by $F_c = 4(f_{Sb}-f_{In})$ where f_{Sb} and f_{In} are the atomic scattering factors of antimony and indium atoms, respectively. Since these structure factors involve the difference in the scattering factors of constituent atoms, the expected experimental structure factors will be weak. We have made a study on the electron density and bonding without and with the inclusion of the quasi-forbidden reflections in this work.

3.2. Electron Density Using MEM

The very important statistical approach to deal with various crystallographic problems is the maximum entropy method (MEM) introduced by Collins [8]. MEM gives less biased information on the electron densities. Currently, this formalism is used as an effective tool to obtain qualitative as well as quantitative electron density distribution of atoms in crystalline materials. It

Table 1. Structure factors of InSb refined using JANA 2006.

h	k	l	F_o	F_c	$\sigma(F_o)$
−1	1	1	350.53	347.51	3.57
1	1	1	351.52	348.07	3.58
0	0	2	29.39	17.52	0.97
−2	2	2	19.43	23.96	1.57
0	2	2	463.88	444.13	4.64
2	2	2	19.70	22.87	1.57
−1	1	3	357.88	374.26	3.62
1	1	3	356.39	373.08	3.61
−3	3	3	334.79	347.77	3.58
−1	3	3	347.99	351.05	3.54
1	3	3	351.35	352.49	3.57
3	3	3	336.81	346.38	3.60
0	0	4	452.78	456.80	4.61
−2	2	4	446.97	445.14	4.53
0	2	4	33.20	26.89	0.68
2	2	4	450.99	445.18	4.57
−4	4	4	394.19	391.62	4.53
−2	4	4	33.72	42.44	1.49
0	4	4	432.88	426.85	4.54
2	4	4	33.43	40.90	1.51
4	4	4	392.99	391.83	5.05
−1	1	5	332.34	331.85	3.42
1	1	5	335.29	333.36	3.45
−3	3	5	298.27	278.56	3.23
−1	3	5	317.49	322.54	3.27
1	3	5	315.85	321.05	3.26
−3	3	5	301.02	280.31	3.25
−3	5	5	272.04	302.23	3.36
−1	5	5	283.62	271.89	3.13
1	5	5	285.99	273.63	3.15
3	5	5	271.15	300.76	4.38
−2	2	6	45.20	39.47	1.47
0	2	6	411.82	407.73	4.25
2	2	6	29.02	38.32	1.71
−2	4	6	376.11	374.46	3.89
0	4	6	27.49	35.71	1.72
2	4	6	376.75	374.63	3.88
−1	1	7	287.12	286.49	3.21
1	1	7	282.99	284.86	3.18
−1	3	7	268.56	260.91	2.98
1	3	7	267.42	262.69	3.18

produces the so-called 'super resolution' electron density distributions [14].

In this work on InSb, the MEM refinements were carried out by dividing the unit cell into $128 \times 128 \times 128$ pixels. The initial electron density at each pixel is fixed uniformly as $F_{000}/a_0^3 = 1.478\ \mathrm{e}/\mathrm{\AA}^3$, where F_{000} is the total number of electrons in the unit cell and a_0 is the cell parameter. The Lagrangian parameter is suitably chosen so that the convergence criterion $C = 1$ is reached after a minimum number of iterations. For the numerical MEM computations, the software package PRIMA [15] was used. For the 1D, 2D, and 3D representation of the electron densities, the program VESTA [16] package was used. The MEM parameters are given in Table 2. The 3D electron density distribution in the form of iso-surface in the unit cell is represented in Figure 2a and 2b, respectively, for the analysis with and without $h+k+l = 4n+2$ reflections. The 2D electron density distribution for the reflections with and without $h+k+l = 4n+2$ on the (110) plane is given in Figure 3a and 3b. Similarly, the 2D density distribution on the (100) plane is shown in Figure 4a and 4b, respectively. The one-dimensional electron density profiles for the analysis of reflections with and without $h+k+l = 4n+2$ reflections, along [100], [110], and [111] directions are represented in Figure 5a and 5b, respectively. Tables 3 and 4 give the numerical values of the electron densities along the three crystallographic directions [100], [110], and [111].

Table 2. Parameters used and obtained in MEM refinements.

Parameter	With $h+k+l = 4n+2$	Without $h+k+l = 4n+2$
Number of cycles	1064	5160
Lagrange parameter (λ)	0.022	0.006
Prior electron density ($\mathrm{e}/\mathrm{\AA}^3$)	1.478	1.478
R_{MEM} (%)	1.9	1.6
wR_{MEM} (%)	2.3	2.0
Resolution (Å)	0.05	0.05

Table 3. 1D electron density of InSb (with $h+k+l = 4n+2$ type reflections) along the three directions in the unit cell.

Direction	Position (Å)	Density ($\mathrm{e}/\mathrm{\AA}^3$)
[100]	0.000	894.5500 (In peak)
[100]	3.232	0.0136
[100]	6.463	894.5500
[110]	2.285	0.1949
[111]	1.399	0.2564 (Mid-bond)
[111]	2.798	1289.7100 (Sb peak)

Table 4. 1D electron density of InSb (without $h+k+l = 4n+2$ type reflections) along the three directions in the unit cell.

Direction	Position (Å)	Density ($\mathrm{e}/\mathrm{\AA}^3$)
[100]	0.000	981.8100 (In peak)
[100]	3.231	0.0137
[100]	6.463	981.8100
[110]	2.285	0.2377
[111]	1.399	0.2632 (Mid-bond)
[111]	2.788	1182.9000 (Sb peak)

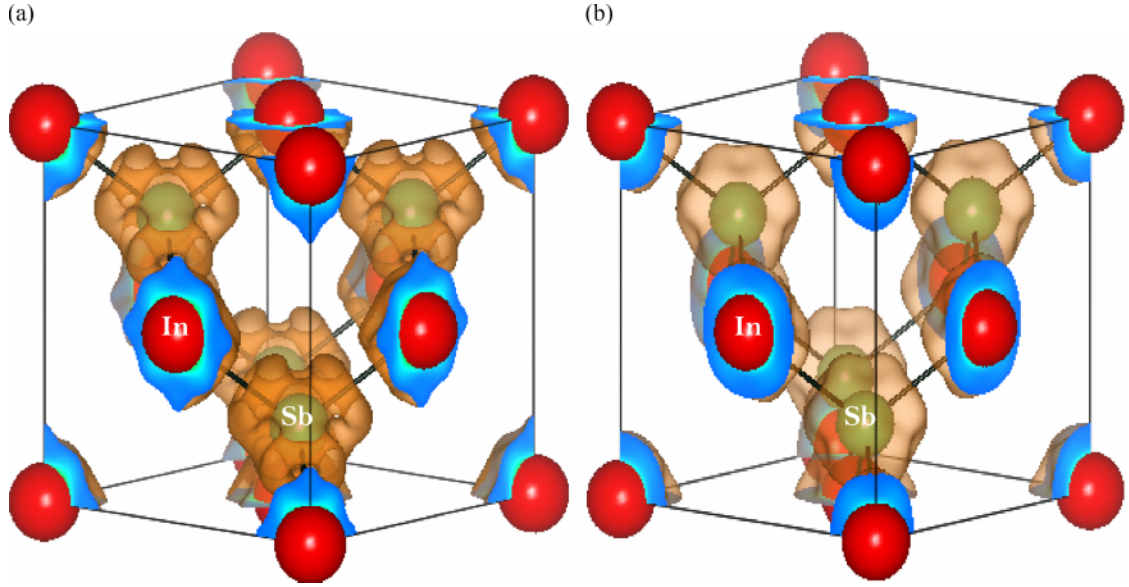

Fig. 2 (colour online). (a) 3D iso-surface of the electron density of InSb in the unit cell (analysis with $h+k+l=4n+2$ reflections); (b) 3D iso-surface of the electron density of InSb in the unit cell (analysis without $h+k+l=4n+2$ reflections).

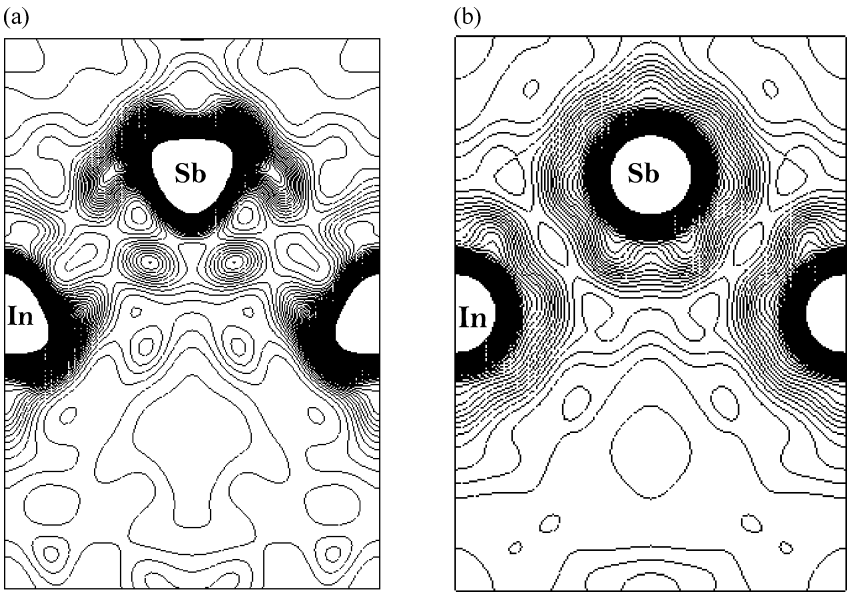

Fig. 3. (a) MEM electron density contour map of InSb on (110) plane (analysis with $h+k+l=4n+2$ reflections); (b) MEM Electron density map of InSb on (110) plane (analysis without $h+k+l=4n+2$ reflections).

4. Results and Discussion

The analyzed structure factors using [13], as seen from Table 1, show a close matching of observed and calculated structure factors. The reliability indices are low indicating the completeness of the refinement procedures.

The 3D electron density distribution of InSb as seen from Figures 2a and 2b show the bonding between In and Sb atoms and the interaction of electron clouds of these atoms. Though there are minute differences in the electron density distributions when the quasi-forbidden reflections are included or excluded from the analysis, the interactions of the

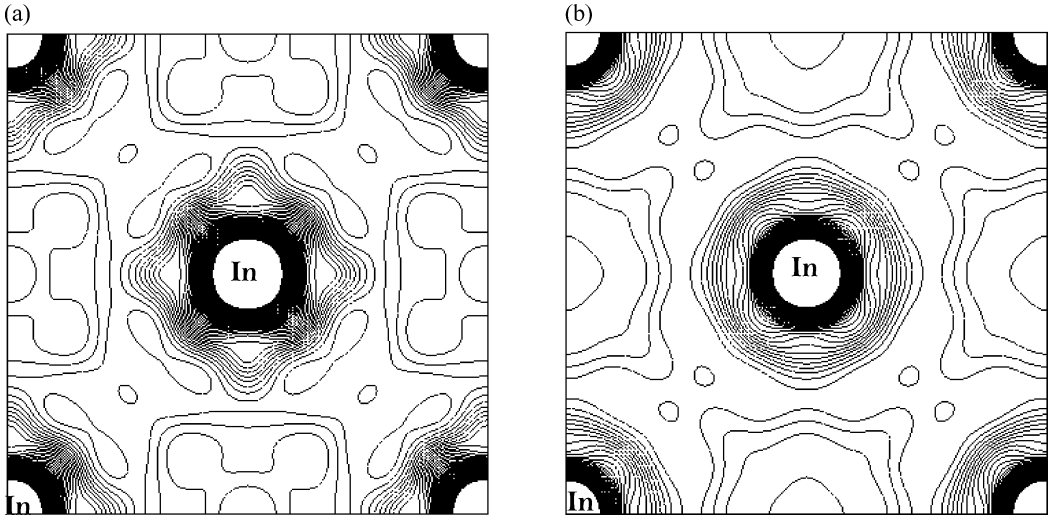

Fig. 4. (a) MEM electron density map of InSb on (100) plane (analysis with $h+k+l=4n+2$ reflections); (b) MEM electron density map of InSb on (100) plane (analysis without $h+k+l=4n+2$ reflections).

In and Sb atoms are the same in general, in both cases.

The two dimensional electron density distributions on the (110) plane with $h+k+l=4n+2$ and without $h+k+l=4n+2$ type reflections as shown in Figures 3a and 3b, evidence a strong covalent interaction between the In and Sb atoms. Since InSb belongs to face-centered cubic (FCC) structure, the two dimensional electron density distribution on the (100) plane (Figs. 4a and 4b), both with $h+k+l=4n+2$ and without $h+k+l=4n+2$ type reflections, show the distribution of In atoms only. When the $h+k+l=4n+2$ type reflections are excluded, the electron clouds show symmetric and uniformly distributed pattern, both in (100) and (110) planes.

The one-dimensional electron density profiles along the (100), (110), and (111) directions of the unit cell of InSb with $h+k+l=4n+2$ and without $h+k+l=4n+2$ type reflections are shown in Figures 5a and 5b for the low density region. The one-dimensional electron density values along the bonding direction [111] with $h+k+l=4n+2$ and without $h+k+l=4n+2$ type reflections reveal a mid bond electron density of $0.2564\,\mathrm{e}/\mathrm{\AA}^3$ and $0.2632\,\mathrm{e}/\mathrm{\AA}^3$, respectively, between In and Sb atoms at a distance of 1.399 Å from the origin. This indicates the covalent nature of InSb and proves that InSb is a very good thermoelectric material due to heavy charge concentration but with a localized nature. The 2D electron density distributions also support the localized charge distribution in InSb.

5. Conclusion

The present analysis visualizes the internal structure and the electron density distributions of the thermoelectric material indium antimonide. The electron density study clearly reveals the covalent interactions between indium and antimony atoms along the bonding direction [111]. In addition to the covalent nature, heavy charge concentration with localized nature supports the thermoelectric character in InSb. Robert and Saravanan [17] have studied that the enhancement of the electron density in $Bi_{80}Sb_{20}$ can give high electrical conductivity. For a thermoelectric material, phonon glass and electron crystal (PGEC) behaviour is essential. A PGEC material features cages (or tunnels) in crystal structure inside which reside atoms small enough to rattle, i.e., to create dynamic disorder. This situation produces a phonon damping effect which results in a reduction of the solid lattice thermal conductivity [17]. In $Bi_{80}Sb_{20}$ the 2D MEM electron density maps of Bi, Sb on the (110) plane show that though there are open channels (voids) in Sb and Bi for higher lattice vibrations, there is much less space for the atoms to contribute lattice vibration in $Bi_{80}Sb_{20}$. This is one

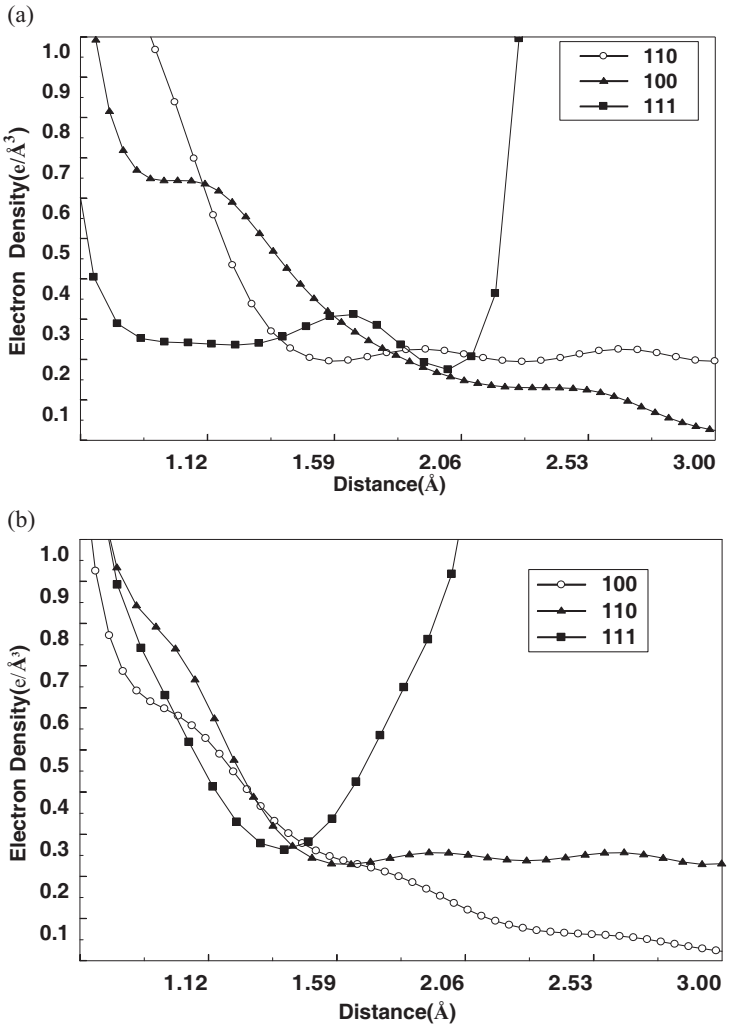

Fig. 5. (a) One dimensional MEM electron density profiles of InSb along [100], [110], and [111] directions (analysis with $h+k+l=4n+2$ reflections); (b) One dimensional MEM electron density profiles of InSb along [100], [110], and [111] (analysis without $h+k+l=4n+2$ reflections).

way to increase ZT by minimizing the lattice thermal conductivity, while retaining good electrical and thermo power properties. In Mg_2Si thermoelectric material [18] too, similar behaviour of covalent bonding mixed with some ionic nature has been found. Similar charge density behaviour is observed in the present case justifying InSb as a good thermo electric material too.

[1] J. P. Fleurial, G. J. Synder, J. Patel, J. A. Herman, T. Caillat, B. Nesmith, and E. A. Kolawa, Jet Propulsion Laboratory/California Institute of Technology MS 277-207, 4800 Oak Grave drive, Pasadena, California 91109, USA Vol. 818, p. 354, 2001.
[2] G. A. Slack, CRC Handbook of Thermoelectrics, ed. by D. M. Rowe, CRC Press, Boca Raton, FL, 1995.
[3] J. Xu and H. Kleinke, J. Comput. Chem. **29**, 2134 (2008).
[4] J. H. Seol, A. L. Moore, S. K. Saha, F. Zhou, and L. Shi, J. Appl. Phys. **101**, 23706 (2007).
[5] S. K. J. Al-Ani, Y. N. Obaid, S. J. Kasim, and M. A. Mahdi, Int. J. Nanoelectron. Mater. **2**, 99 (2009).
[6] M. Matsumoto, J. Yamazki, and S. Yamaguchi, Mater. Res. Soc. Symp. Proc. 0980-II05-42 (2007).

[7] Q. Wang, X. M. Chen, and K. Q. Lu, J. Phys.: Condens. Matter **12**, 5201 (2000).
[8] D. M. Collins, Nature **298**, 49 (1982).
[9] H. M. Rietveld, J. Appl. Cryst. **2**, 65 (1969).
[10] S. Israel, R. Saravanan, N. Srinivasan, and R. K. Rajaram, J. Phys. Chem. Solids **64**, 43 (2003).
[11] S. Israel, R. Saravanan, and R. K. Rajaram, Physica B **349**, 390 (2004).
[12] M. Sakata and M. Sato, Acta Cryst. A **42**, 263 (1990).
[13] V. Petříček, M. Dušek, and L. Palatinus, JANA 2000, The crystallographic computing system, 2000.
[14] R. Saravanan, Y. Ono, M. Isshikic, K. Ohno, and T. Kajitani, J. Phys. Chem. Solids **64**, 51 (2003).
[15] F. Izumi and R. A. Dilanian, "Recent Research Developments in Physics", Vol. 3, Part II, Transworld Research Network, Trivandrum, p. 699 (2002).
[16] K. Momma and F. Izumi, J. Appl. Crystallogr. **41**, 653 (2008).
[17] M. C. Robert and R. Saravanan, Powder Technol. **197**, 159 (2010).
[18] R. Saravanan and M. C. Robert, J. Alloys Compd. **479**, 26 (2009).